Title
Reactive Transport Model of Sulfur Cycling as Impacted by Perchlorate and Nitrate Treatments

Journal
Environmental Science and Technology, 50(13)

ISSN
0013-936X

Authors
Cheng, Yiwei
Hubbard, Christopher G
Li, Li
et al.

Publication Date
2016-07-05

DOI
10.1021/acs.est.6b00081

Peer reviewed

Environmental Science & Technology

Article

pubs.acs.org/est

Reactive Transport Model of Sulfur Cycling as Impacted by Perchlorate and Nitrate Treatments

Yiwei Cheng,*[,†] Christopher G. Hubbard,[†] Li Li,[‡] Nicholas Bouskill,[†] Sergi Molins,[†] Liange Zheng,[†] Eric Sonnenthal,[†] Mark E. Conrad,[†] Anna Engelbrektson,[§] John D. Coates,[§] and Jonathan B. Ajo-Franklin[†]

[†]Lawrence Berkeley National Laboratory, Berkeley, California, 94720 United States

[‡]Pennsylvania State University, University Park, Pennsylvania, 16802 United States

[§]Department of Plant and Microbial Biology, University of California, Berkeley, California, 94720 United States

Supporting Information

ABSTRACT: Microbial souring in oil reservoirs produces toxic, corrosive hydrogen sulfide through microbial sulfate reduction, often accompanying (sea)water flooding during secondary oil recovery. With data from column experiments as constraints, we developed the first reactive-transport model of a new candidate inhibitor, perchlorate, and compared it with the commonly used inhibitor, nitrate. Our model provided a good fit to the data, which suggest that perchlorate is more effective than nitrate on a per mole of inhibitor basis. Critically, we used our model to gain insight into the underlying competing mechanisms controlling the action of each inhibitor. This analysis suggested that competition by heterotrophic perchlorate reducers and direct inhibition by nitrite produced from heterotrophic nitrate reduction were the most important mechanisms for the perchlorate and nitrate treatments, respectively, in the modeled column experiments. This work demonstrates modeling to be a powerful tool for increasing and testing our understanding of reservoir-souring generation, prevention, and remediation processes, allowing us to incorporate insights derived from laboratory experiments into a framework that can potentially be used to assess risk and design optimal treatment schemes.

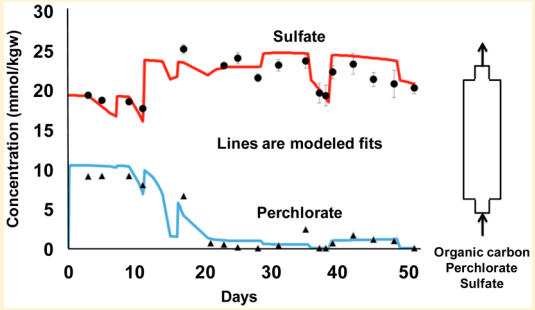

INTRODUCTION

Reservoir souring is the production of hydrogen sulfide (H_2S) from thermochemical or biogenic sulfate reduction in oil fields.[1] Hydrogen sulfide poses significant health and environmental risks,[2] and its corrosive nature compromises the structural integrity of production facilities.[3] Sulfides also lower the quality and profit margin of oil by ∼10%.[4] Thermochemical production of H_2S occurs typically at temperatures of 100−180 °C, whereas biogenic production by sulfate reducing microorganisms (SRM, i.e., bacteria and archaea) occurs below this temperature.[1] Microbial souring is most pronounced during secondary oil recovery, where the injection fluid used to maintain pressure and sweep oil is often seawater. Seawater contains a high sulfate concentration (28 mM), stimulating the growth and activity of SRM.

Prevention of reservoir souring has focused primarily on inhibiting the growth and activity of SRM using biocide. A common alternative is the injection of nitrate.[5−7] Nitrate inhibits souring either by fostering competition between the heterotrophic nitrate reducers (hNRM) and SRM for electron donors or through the production of an intermediate, nitrite, that inhibits SRM.[8] Furthermore, nitrate can also stimulate further sulfide oxidation through nitrate reducing, sulfide oxidizing microorganisms (NR-SOM)[9,10] (Figure 1B). Perchlorate injection has recently been demonstrated as an alternative to nitrate injection.[11−13] Perchlorate inhibits sulfide production through multiple mechanisms (Figure 1A), including competition between perchlorate reducers (PRM) and SRM for electron donors, and inhibition of SRM by perchlorate.[14] PRM can also couple the oxidation of sulfide to the reduction of perchlorate, removing sulfide as elemental sulfur.[12]

These complex biogeochemical processes are often coupled with flow and transport processes under reservoir conditions. Process-based models provide a tool with which to differentiate the importance of competing processes while at the same time offering a systematic view that integrates disparate processes and data sets. Empirical models for reservoir souring have existed for more than two decades.[15,16] The development of mechanism-based reservoir souring models with a complex representation of key biogeochemical processes coupled with multiphase flow simulators, however, has been relatively recent.[10,17,18] An example is UTCHEM,[18] a multicomponent reservoir model that includes a biological souring module for the simulation of nitrate amendments by explicitly taking into

Received: January 8, 2016
Revised: May 31, 2016
Accepted: June 6, 2016
Published: June 6, 2016

DOI: 10.1021/acs.est.6b00081
Environ. Sci. Technol. 2016, 50, 7010−7018

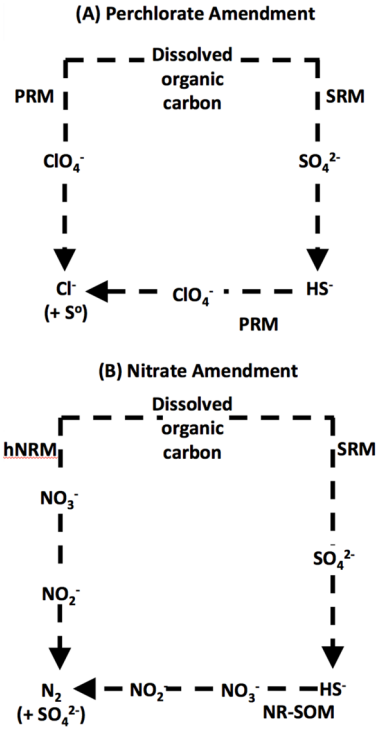

Figure 1. Kinetically controlled microbial reactions and the formation of biomass during (A) perchlorate amendment and (B) nitrate amendment. PRM, perchlorate reducing microorganisms; SRM, sulfate reducing microorganisms; hNRM, heterotrophic nitrate reducing microorganisms; and NR-SOM, nitrate reducing sulfide oxidizing microorganisms.

account the growth of SRM, hNRM, and NR-SOM.[19] To our knowledge, no process-based models have been developed to understand perchlorate as an inhibitor of sulfide production. As a result, the relative importance of individual inhibition mechanisms involved in the perchlorate inhibition of sulfidogenesis remains elusive.

The objective of this paper is to understand controlling mechanisms during souring treatments. Specifically, we aim to uncover the role of individual mechanisms for perchlorate and nitrate amendments, teasing out the relative importance of competition, inhibition, and sulfide reoxidation. To achieve this, we develop the first model of perchlorate inhibition of microbial sulfate reduction and validate our reaction networks for perchlorate and nitrate using data from recent columns experiments.[11] Sulfur isotopes are integrated into the model for additional constraints on the timing and magnitude of microbial sulfate reduction.[20−22] Sensitivity analysis is used to explore the role of individual mechanisms in influencing sulfide production. Lastly, we discuss implications for field treatment and suggest future directions to constrain and improve modeling of reservoir souring and souring-treatment processes.

MATERIALS AND METHODS

Description of Column Experiments. The modeled biogeochemical reaction network was validated using column data from Engelbrektson et al.[11] This is the only published set of column experiments to compare the effectiveness of perchlorate against nitrate amendments in inhibiting H_2S production and, as such, is the best available data set for our modeling study. Sealed 50 mL glass syringes were used as flow-through columns. The columns were packed with a mixture of 50% San Francisco Bay sediment (microbial inoculum) and 50% glass beads (70−100 μm diameter), which resulted in a porosity of ∼0.33. The injection fluid was water from the San Francisco Bay (19−33 mM sulfate) with 1 g/L yeast extract (labile carbon source) and 10 mM of treatment chemical (sodium nitrate, sodium perchlorate, or no treatment control, all performed in triplicate). The effect of amendment concentration was explored by decreasing concentrations to 5 mM for 3 days on day 35 before returning to 10 mM. A total of two flow regimes were prescribed throughout the experiment (Figure 2). For the first 28 days, flow was intermittent, with periods of flow (at a rate of 0.1 mL/min) and no flow. For the remainder of the experiment (days 29−51), flow was continuous at 0.025 mL/min. Engelbrektson et al.[11] demonstrated that perchlorate effectively inhibited sulfate reduction. In contrast, nitrate inhibited sulfate reduction for the first 23 days, after which sulfate reduction continued at significant rates following the complete consumption of nitrate. Sulfur isotope ratios of dissolved sulfate samples from each treatment were reported in standard delta notation relative to the Canyon Diablo Troilite standard (R_{std} = 0.0441216) as $\delta^{34}S$ (‰) = $(R_{sample}/R_{std} - 1) \times 1000$, where $R = {}^{34}S/{}^{32}S$.

Reactive Transport Modeling. Reactive transport models (RTM) solve equations that describe coupled fluid flow, mass transport, and biogeochemical processes in subsurface environments. RTMs have been applied to problems in geologic emplacement of high-level nuclear waste,[23,24] contaminant remediation,[21,25,26] and geological CO_2 sequestration.[27−30] A general reactive transport equation for a chemical species i is as follows:[31]

$$\frac{\partial(\phi S_L C_i)}{\partial t} = \nabla\cdot(\phi S_L D_i \nabla C_i) - \nabla\cdot(qC_i) - \sum_{j=1}^{Nj} \nu_{ij} R_j - \sum_{l=1}^{Nl} \nu_{il} R_l - \sum_{m=1}^{Nm} \nu_{im} R_m \quad (1)$$

where the term on the left side is the mass accumulation rate (mol/s), and the terms on the right side are diffusion and dispersion, advection terms, and reaction terms: aqueous-phase reactions, R_j; mineral reactions, R_l; and gas reactions, R_m. N_x (where $x = j$, l, or m) represents the total number of reactions (aqueous, mineral, and gas phase, respectively) that involve i, and ν_{ix} represents the stoichiometric coefficient of i associated with reaction x. Here ϕ is porosity, S_L is liquid saturation, C_i is concentration (mole per cubic meter water), D is the diffusion and dispersion coefficient (m^2/s), and q is the Darcy flux.

In this work, we used the multicomponent, multiphase reactive-transport simulator, TOUGHREACT,[32,33] which used the integrated finite-difference form of the species mass conservation equation shown in eq 1. Details of the treatment of the biogeochemical reactive-transport equations and coupling with nonisothermal multiphase fluid flow have been published previously.[33−36] We extended TOUGHREACT applications to modeling isotopic[26,37] and biogeochemical systems[34] by explicitly representing the kinetics of individual sulfate isotopologues, i.e., $^{32}SO_4^{2-}$ and $^{34}SO_4^{2-}$, with a modified dual Monod rate expression, following the approach taken in the reactive transport model CRUNCHTOPE.[20] The major bioreduction reactions and microbes represented are shown in Figure 1. Modeled microbially mediated reactions are divided into two components: catabolic and anabolic. For each mole of electron donor and substrate utilized, a fraction, f_s, is conserved

DOI: 10.1021/acs.est.6b00081
Environ. Sci. Technol. 2016, 50, 7010−7018

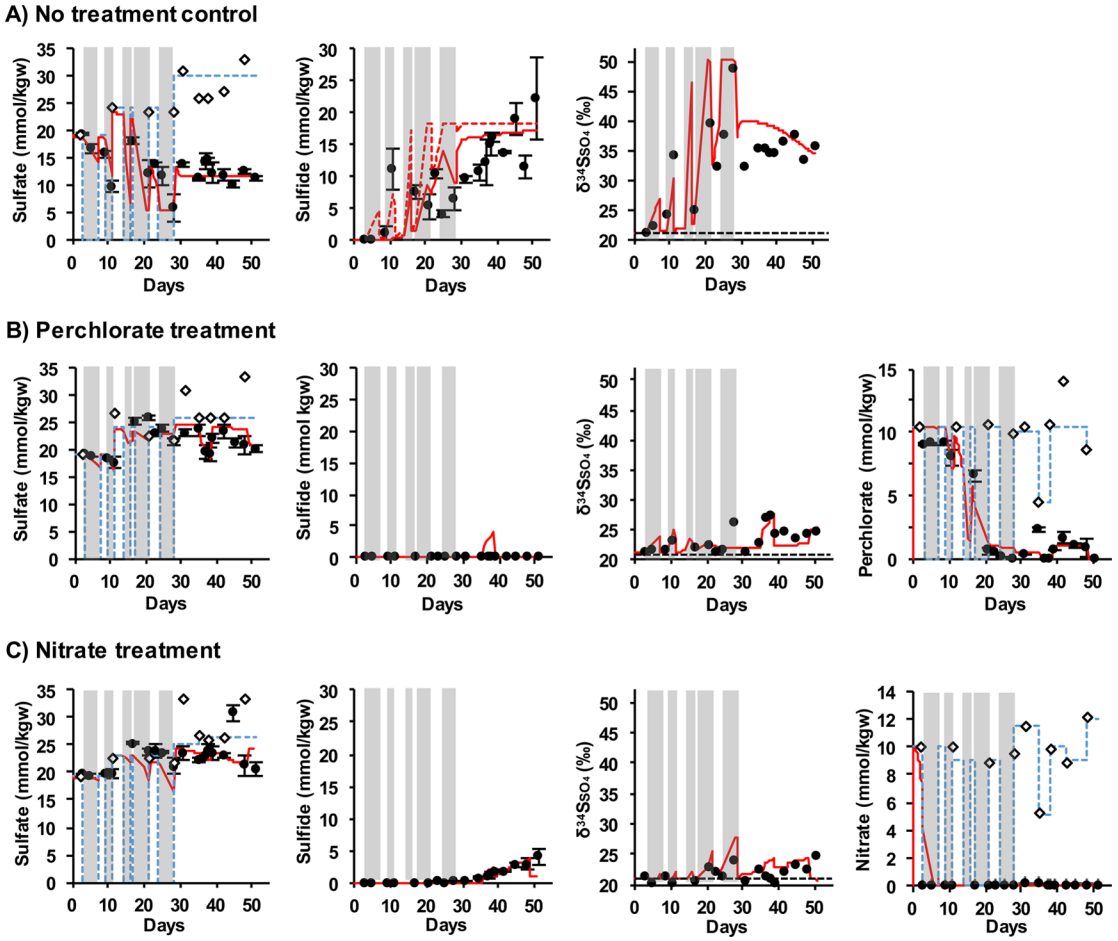

Figure 2. Model data comparison: (A) no treatment; dashed red line is model output of sulfide concentration when iron minerals are not included. Dashed black lines (δ^{34}S graphs) show influent sulfate value. (B) Perchlorate treatment; (C) nitrate treatment. Open diamonds are influent data points, and filled circles are effluent data (error bars are 1σ, n = 3) from Engelbrektson et al.[11] Solid red lines are model fits to the data. Dashed blue lines (sulfate, perchlorate, and nitrate concentration graphs) are model influent values. Gray shaded areas correspond to periods of no flow.

by the microbial biomass for cell synthesis (anabolic), while the remaining fraction, f_e, is used for energy production (catabolic). Detailed reaction stoichiometries are written based on the bioenergetics concept[38] (Table S1). Kinetics of these reactions follows Monod formulation:

$$r = \mu[\text{Biomass}]\frac{[\text{eDonor}]}{[\text{eDonor}] + K_{\text{eDonor}}} \frac{[\text{eAcceptor}]}{[\text{eAcceptor}] + K_{\text{eAcceptor}}} \frac{K_{\text{Inhibitor}}}{[\text{Inhibitor}] + K_{\text{Inhibitor}}} - m[\text{Biomass}] \quad (2)$$

where r (mol/kgw/sec) is the reaction rate (kgw = kg of water), [Biomass] (mol/kgw) is the concentration of the microbial biomass, μ (sec^{-1}) is the maximum specific growth rate, K_e (mol/kgw) is the half saturation (affinity constant) of the electron donor and acceptor, $K_{\text{Inhibitor}}$ is the inhibitor constant (mol/kgw), and m (sec^{-1}) is a decay and mortality constant. Note that the inhibition term is close to one, meaning no inhibition effects when $K_{\text{Inhibitor}} \gg$ [Inhibitor]. This means that larger $K_{\text{Inhibitor}}$ means lower inhibition effects in the system.

Following the general rate expression in Maggi and Riley[39] and the recent implementation in a reactive transport model (CRUNCHTOPE),[20] sulfate reduction rates of different isotopologues are expressed as follows:

$$^{32}r = {}^{32}\mu[\text{SRM}]\frac{[^{32}SO_4^{2-}]}{[SO_4^{2-}] + K_S^{SO_4}} \times \frac{[\text{eDonor}]}{[\text{eDonor}] + K_S^{\text{eDonor}}} \times \frac{K_S^{\text{Inhibitor}}}{[\text{Inhibitor}] + K_S^{\text{Inhibitor}}} \quad (3)$$

$$^{34}r = {}^{34}\mu[\text{SRM}]\frac{[^{34}SO_4^{2-}]}{[SO_4^{2-}] + K_S^{SO_4}} \times \frac{[\text{eDonor}]}{[\text{eDonor}] + K_S^{\text{eDonor}}} \times \frac{K_S^{\text{Inhibitor}}}{[\text{Inhibitor}] + K_S^{\text{Inhibitor}}} \quad (4)$$

where [SRM] is the concentration of SRM. Equations 3 and 4 follow the general formulation presented in equation 2. When sulfate coexists with inhibitors such as perchlorate and nitrite, the inhibition terms in equations 3 and 4 includes constants $K_{In}^{ClO_4}$ and $K_{In}^{NO_2^-}$, respectively. The fractionation factor (α) can be calculated as $\alpha = \frac{^{34}\mu}{^{32}\mu}$

In our simulation, we represent the electron donor (1 g/L yeast extract) as 20 mM acetate. This is a simplification because yeast extract is a complex electron donor that can be broken down into multiple intermediates, and different microbial populations may have different affinities for these intermediates. This is analogous to crude oil in a reservoir, which is also a

DOI: 10.1021/acs.est.6b00081
Environ. Sci. Technol. 2016, 50, 7010−7018

complex donor. However, without additional experimental data on intermediates, a simplification is needed, both in this simulation and in the modeling of oil reservoir souring. Acetate (and other volatile fatty acids) is often used to model microbial souring. A simple anaerobic bottle experiment with San Francisco Bay water, sediment, and yeast extract showed that 1 g/L yeast extract reduced 18.2 mM sulfate, equivalent to ~20 mM of acetate according to our reaction stoichiometry (Table S2). Yeast extract typically contains 10−11 wt % N. For 1 g/L yeast extract, this is equivalent to 7.5 mM N, represented in our simulation as NH_4 (Tables S1 and S2) and used for microbial growth. Note that NH_4 was in excess in all our simulations with ≤4.6 mM consumed.

Results from the column experiment revealed a delay in sulfide breakthrough in comparison to the $\delta^{34}S$ trend, suggesting the presence of iron mineral−sulfide reactions. We modeled this sink as reaction with iron minerals (Tables S2 and S3).[20,21,25,44−46] The iron mineralogy in the sediment was not explicitly determined and is likely to be a combination of iron-bearing clays and iron (oxyhydr)oxides. For modeling simplicity, we represented it as a single $Fe(OH)_3$ phase with an assumed surface area of 40 m^2/g and log K of −10.0 (consistent with goethite[44]). The initial mineral quantity of 0.1% corresponds to the amount of iron contributed by the San Francisco Bay sediment, as determined by a 6 M hydrochloric acid leach.[47] This combination of parameters provided a reasonable fit to the data. The reactions represented here followed previously published reaction networks.[20,21,25,46] Rates of mineral dissolution and precipitation are calculated based on a rate law derived from transition-state theory.

Model Setup. The columns are modeled as 1D systems of approximately 0.12 m (height of columns) discretized into 120 grid blocks of 0.001 m. The sequence of flow rates from the experiments was used in the model. The diffusion coefficient was set to 1.83×10^{-9} m^2/s, within the range of experimental values.[40] We simulate three sets of triplicate columns with different inlet-fluid composition depending on the type of treatment (Table S1). All reactions and their kinetic and thermodynamic parameters are listed in Tables S2 and S3.

The no-treatment column data were reproduced first to obtain parameters relevant to sulfate reduction, including SRM growth rate, half-saturation constants, iron−sulfide mineral kinetics, and isotope fractionation factor. These values were then used for perchlorate- and nitrate-treatment simulations to ensure consistency. The nitrate- and perchlorate-column simulations were fitted to the data by varying parameters pertaining to hNRM, NR-SOM, and PRM. Gregoire et al.[12] showed that perchlorate reducers preferentially use sulfide to labile carbon as the electron donor but do not grow significantly in this mechanism. To model this, we used the same PRM population to mediate both heterotrophic perchlorate reduction and perchlorate-reduction sulfide oxidation (Tables S2 and S3), with a sulfide inhibition constant applied to heterotrophic perchlorate reduction (Table S4). For nitrate, we modeled NRM and NR-SOM separately. For each group, the reduction of nitrate was split into two parts: (1) $NO_3^- \rightarrow NO_2^-$, and then (2) $NO_3^- \rightarrow N_2$. This allowed us to model the inhibitory effect of nitrite on sulfate reduction. No measurements of initial microbial population sizes were made by Engelbrektson et al.[11] Following the approach of previous modeling studies,[20,21] we started with an initial homogeneous distribution of biomass at a low concentration (Table S5). Note that PRM initial biomass was set an order of magnitude lower, reflecting the lower abundance of PRM in the environment.

RESULTS AND DISCUSSION

No-Treatment Columns. In the column experiment influent sulfate concentrations varied between 19.0 and 33.7 mM (Figure 2), depending on when the batches of water samples used in the experiment were collected from the San Francisco Bay.[11] The model captured the timing of the observed effluent sulfate concentrations (Figure 2A), along with the rise in sulfide concentration data. In general, the increase in sulfide concentration mirrored the decrease in sulfate concentration. The fluctuation in sulfate and sulfide concentrations in the first 30 days is due to the intermittent flow pattern with periods of no flow. During the shutoff period, modeled effluent sulfate concentration decreased (the gray shaded area in Figure 2A) in response to microbial sulfate reduction and no sulfate influx. When flow was resumed, effluent sulfate concentrations spiked up because sulfate reduction rates were relatively low compared to the sulfate influx. The model captured the rise in $\delta^{34}S$ throughout the experiment. Values of $\delta^{34}S$ greater than the influent seawater signal of 21‰ (dashed black line) correspond to the decrease in effluent sulfate concentrations relative to influent values and represent microbial sulfate reduction. SRM preferentially reduce the lighter ^{32}S, leading to a progressive increase in the $\delta^{34}S$ of remaining sulfate. The kinetic fractionation factor, α, used in this study was 0.9748, within the range of 0.9579−0.9870 used in previous studies.[20,21,41−43]

The data revealed a delay in sulfide breakthrough in comparison to changes in effluent sulfate and $\delta^{34}S$ values (Figure 2A), interpreted as iron mineral−sulfide reactions.[11] Delays in effluent sulfide had previously been observed in other field[20] and column studies[21] that emphasized the value of using $\delta^{34}S$ as a proxy for onset of sulfate reduction.[20−22] The observed effluent sulfate and $\delta^{34}S$ pointed toward the occurrence of sulfate reduction as early as the first shutoff period (days 3−7, Figure 2A). The effluent sulfate concentration decreased by as much as 4.0 mmol/kgw, and $\delta^{34}S$ increased by 4.0‰ by the end of this period. However, no rise in the effluent sulfide concentration was observed during this period, suggesting a sink for sulfide within the column. We modeled this sink as reaction with iron minerals (see the Methods section and Tables S2 and S3[20−22,44−46]). In the absence of the iron mineral−sulfide reactions, sulfide breakthrough mirrored the changes in effluent sulfate and $\delta^{34}S$, as shown by the dashed red line in Figure 2.

Perchlorate Columns. Here, we reproduced observed effluent sulfate, sulfide, $\delta^{34}S$, and perchlorate data. Effluent data indicated the effectiveness of perchlorate in preventing souring (Figure 2B). Effluent sulfide was only produced by the model when influent perchlorate concentration was halved (days 35−38), and effluent sulfate was also reduced relative to influent during this period. Effluent perchlorate decreased after 10 days, indicating significant perchlorate reduction. The departure of $\delta^{34}S$ values from the baseline 21‰ were most noticeable toward the end of the experiment (maximum of ~27‰), suggesting limited SRM activity even when effluent sulfide was not detected.[11]

Nitrate Columns. As with the perchlorate treatment, effluent sulfate concentrations remained similar to influent concentrations during much of the intermittent flow phase. However, after day 20, sulfate reduction proceeded at

DOI: 10.1021/acs.est.6b00081
Environ. Sci. Technol. 2016, 50, 7010−7018

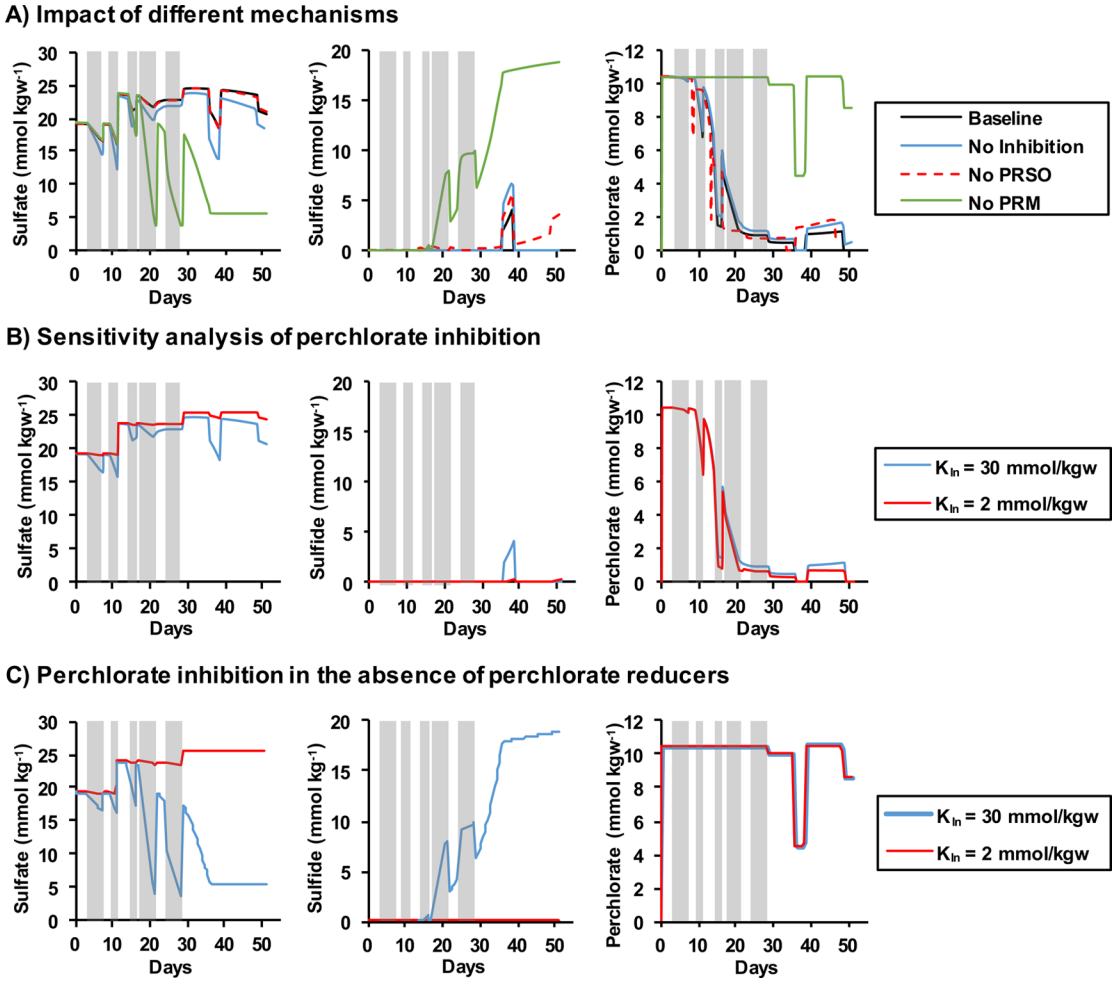

Figure 3. (A) Factorial analysis of the impact of different perchlorate-related mechanisms on sulfate reduction. (B) Sensitivity analysis of the perchlorate inhibition constant (K_{In}) of the sulfate reducers. (C) Sensitivity analysis of the perchlorate inhibition constant (K_{In}) of the sulfate reducers in the absence of perchlorate reducers. Gray shaded areas correspond to periods of no flow.

detectable rates, as indicated by effluent $\delta^{34}S$ and sulfate data. In contrast to the perchlorate treatment, sulfide production steadily increased during nitrate treatment after day 30 and reached a maximum of about 4 mmol/kgw. The model captured the trends of effluent $\delta^{34}S$, nitrate, sulfate, and sulfide (Figure 2C). It underpredicted nitrate reduction rates in the first 5 days; however, it reproduced the data thereafter (Figure 2C). During the intermittent phase, effluent nitrate concentrations remained zero, suggesting rapid nitrate utilization. Observed effluent data suggested that nitrate is a less-effective inhibitor of sulfide production than perchlorate on a per mole of electron-acceptor basis, with higher effluent sulfide values observed in the nitrate experiments. However, it should be noted that according to our reaction-network stoichiometry (Table S2) heterotrophic perchlorate reduction consumes 2.22 mol of acetate per mole of perchlorate, whereas heterotrophic nitrate reduction consumes only 0.50 mol of acetate to reduce 1 mol of nitrate to nitrite and 1.44 mol of acetate to reduce 1 mol of nitrate all the way to N_2. An alternative comparison of the two chemicals' effectiveness as biocompetitive electron acceptors to sulfate would be to compare them on an electron donor equivalent basis. The principle aims of our study, however, are to use the column data to validate our perchlorate reaction network and to tease out the importance of all the mechanisms, not just biocompetition, i.e., to also explore the role of inhibition of sulfate reducers and the role of sulfide reoxidation.

Elucidating Inhibition Mechanisms. A major advantage of RTMs is their capability to interrogate complex systems and identify important mechanisms. In the case of reservoir souring and prevention, this insight is essential to help predict and explain when and where different treatments can be successful. For perchlorate treatment, the following scenarios were explored: (1) no direct inhibitory effect of perchlorate on sulfate reduction, (2) no sulfide oxidation coupled with perchlorate reduction (PRSO), and (3) no PRMs. For the first scenario, we removed the inhibition term in eq 2 while leaving the remaining parameters the same as in the baseline perchlorate case shown in Figure 2B and described earlier. For the second scenario, we removed reactions 4 and 5 from Table S2. For the third scenario, we removed reactions 3−5 from Table S2. Effluent sulfate, sulfide, and perchlorate concentrations from each of the scenarios were compared to the baseline perchlorate case. Simulation results (Figure 3A) showed that suppressing sulfide oxidation (no PRSO) made only minor differences to modeled results, with sulfide increasing toward the end of the simulation compared with the baseline. In comparison, removing all PRM activity resulted in much greater microbial sulfate reduction and sulfide generation than that shown in the baseline scenario and

DOI: 10.1021/acs.est.6b00081
Environ. Sci. Technol. 2016, 50, 7010−7018

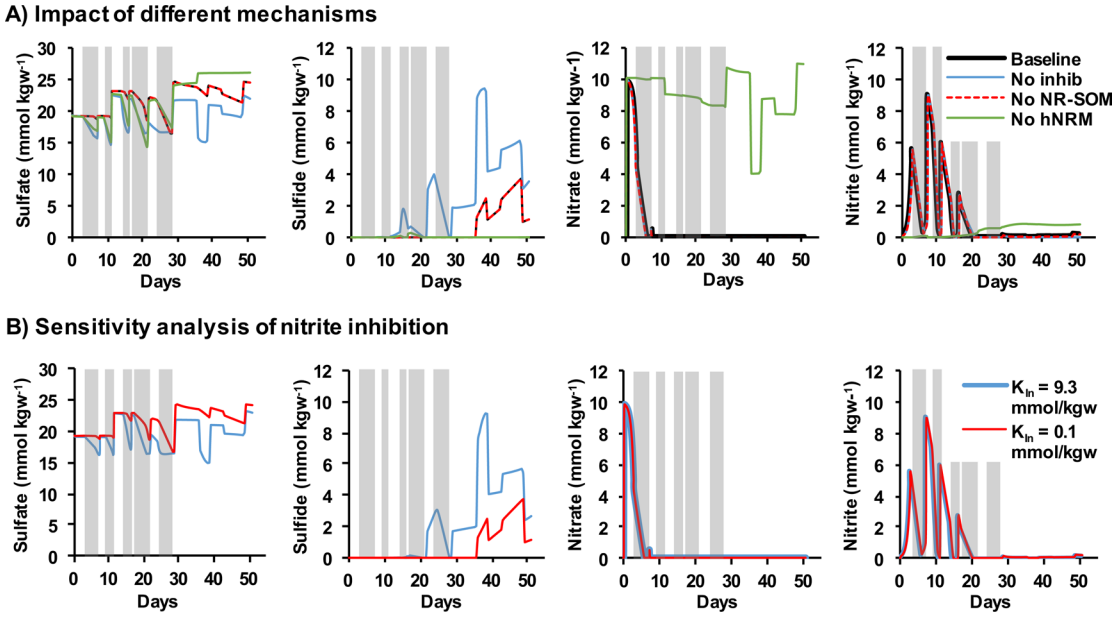

Figure 4. (A) Factorial analysis of the impact of different nitrate-related mechanisms on sulfate reduction. (B) Sensitivity analysis of the nitrite-inhibition constant (K_{In}) of the sulfate reducers. Gray shaded areas correspond to periods of no flow.

observed experimental data. The model therefore suggests that competition between the PRM and SRM for limited electron donors (biocompetition) was the dominant effect. Removing the perchlorate inhibition term did have a minor impact on modeled sulfate values and peak sulfide values, but in this case, our modeling suggested that biological competition for electron donors was stronger than the inhibition effect.

It is important to compare our model results with the observed changes in microbial composition in the experiments themselves. Engelbrektson et al.[11] performed similarity percentage (SIMPER) tests to determine the operational taxonomic units that contributed to the top 10% of difference between each set of treatment samples and the initial inoculum. These analyses showed that perchlorate did enrich for various members of Firmicutes and Proteobacteria; both of these phyla include previously described (per)chlorate reducers. Specifically, Helicobacteraceae were enriched relative to the no-treatment control; this family includes the known perchlorate reducer *Wolinella succinogenes*. Perchlorate also inhibited known sulfate reducers (Desulfobacteraceae, Desulfovibrionaceae, and Desulfomicrobiaceae) compared to the no-treatment control, demonstrating that inhibition clearly did play a role. Finally, SIMPER analyses suggested that perchlorate enriched for Desulfobulbaceae and Desulfuromonadaceae compared with the no-treatment control. These organisms are known to be capable of sulfide oxidation and elemental sulfur cycling (oxidation, reduction, and disproportionation). There is therefore microbial evidence from Engelbrektson et al.[11] for all three mechanisms of perchlorate impacting microbial sulfate reduction; our modeling suggests that biocompetition was the dominant mechanism, with relatively minor contributions from sulfide oxidation and direct inhibition of sulfate reducers.

To further investigate the role of direct inhibition of perchlorate on sulfate reduction, we conducted sensitivity analysis on the inhibition constant of 2 and 30 mmol/kgw, based on the range determined experimentally by Carlson et al.[14] for a marine enrichment culture and the model organism *Desulfovibrio alaskensis* G20. Through experiments with wild type, transposon pools, and *rex* mutants, these authors' results support the hypothesis that perchlorate directly inhibits the central sulfate reduction pathway. Note that the best-fit inhibition constant from our modeling (Figure 2B) was 30 mmol/kgw, the upper value in this range. Simulation results showed that the higher the inhibition constant the lower the inhibition impacts of perchlorate on sulfate reduction, resulting in more effluent sulfide produced compared to the case with the lower inhibition constant (Figure 3B). Also due to the higher degree of sulfate reduction, less of the electron donor was available for perchlorate reduction, resulting in slightly higher effluent perchlorate.

It should be noted that perchlorate reducers are not as abundant as sulfate reducers, and little is currently known about the perchlorate reducing capacity of microbial populations in oil reservoirs.[13] If this capacity is low, then the role of direct inhibition of SRM by perchlorate will be even more critical. To explore this, we ran simulations with no PRM (and therefore no perchlorate reduction) and with inhibition constants set at 2 and 30 mmol/kgw (Figure 3C). The scenario with a low inhibition constant and no PRM activity effectively suppressed sulfidogenesis and represented the ideal situation, i.e., the delivery of an effective SRM inhibitor that can persist without being degraded. The results show the importance of selecting inhibitor dose rates based on the knowledge of the specific microbial community as well as site logistics for dosing. They also highlight the need for measuring perchlorate inhibition constants for both pure cultures of SRM and oil reservoir communities to make more accurate predictions.

For nitrate treatment, the following scenarios were explored to fully appreciate the role of individual mechanisms: (1) no direct inhibitory effect of nitrite on sulfate reduction, (2) no sulfide oxidation by NR-SOM, and (3) no hNRMs. Simulation results suggested that the main mechanism for inhibiting sulfate reduction in these columns was the direct inhibitory effect of nitrite produced from heterotrophic nitrate reduction (Figure 4A). Microbial community analysis[11] showed that nitrate addition did inhibit a known family of SRM (Desulfobacter-

DOI: 10.1021/acs.est.6b00081
Environ. Sci. Technol. 2016, 50, 7010−7018

aceae) relative to no-treatment controls. It should be noted that nitrite was not directly measured in the experiments by Engelbrektson et al.,[11] and this limitation should be kept in mind when interpreting model results. To further explore the impact of nitrite inhibition on sulfate reduction, we conducted sensitivity analysis using the inhibition constant (nitrite on sulfate reduction) of 0.1 and 9.3 mmol/kgw based on the range determined experimentally by Carlson et al.[14] Note that the best-fit inhibition constant from our first round of modeling (Figure 2C) was 0.1 mmol/kgw, the lowest value of this range. Although the inhibition constant values for nitrite are approximately an order of magnitude lower than for perchlorate, similar trends could be observed: the higher the inhibition constant, the lower the toxicity impact of nitrite on sulfate reduction. As a result, more effluent sulfide is produced compared to the case with a lower inhibition constant (Figure 4B). Previous column experiments,[9,48−50] have also suggested an important role for nitrite inhibition. However, the generation of nitrite is expected to vary depending on the presence of specific nitrate reducing populations, the relative activities of microbial nitrite generation and consumption, and the abiotic reactivity of nitrite with the reservoir mineral matrix. Therefore, the extent of nitrite inhibition is likely reservoir-specific.

Microbial-community analysis by Engelbrektson et al.[11] showed that nitrate addition produced the most distinctive change in the columns, stimulating Proteobacteria, Firmicutes and Tenericutes, all of which contain known nitrate reducers. Simulation results for the case of no sulfide reoxidation were the same as the baseline case (Figure 4A), suggesting that hNRM were more dominant than NR-SOM in our model. However, model results did show that if hNRM are removed or inactive, NR-SOMs can dominate (Figure 4A). In this modeling scenario, initial sulfate reduction occurred, with SRM reducing sulfate to sulfide and NR-SOM then reoxidizing sulfide to sulfate. In our particular simulation, sufficient nitrite was produced by NR-SOM to then inhibit sulfate reduction, limiting the sulfide produced and hence nitrate consumed by NR-SOM. A field-relevant scenario where NR-SOM has been shown to outcompete hNRM is when nitrate was added to a system that already contained sulfide.[51,52] In this case, hNRM are inhibited by sulfide, although we do not model this inhibition effect in the current study because sulfide concentrations only start to increase toward the end of the nitrate experiment and remain relatively low. Theoretically, these microbial dynamics could lead to community succession following the addition of nitrate to remediate a soured reservoir.

Oil-reservoir biogeochemistry is complicated by the presence of multiple carbon sources, potentially resulting in the niche separation of different functional groups (e.g., hNRM and SRM) using different electron donors. Yeast extract is also a complex donor and therefore offers similar experimental advantages to crude oil when compared with more defined donors (e.g., volatile fatty acids) and is also more rapidly degraded than crude oil, making it attractive for proof-of-concept studies. However, care needs to be taken when extrapolating results to crude oil systems, and follow-up experiments are clearly warranted. Each system has its advantages and disadvantages, leading to souring experiments in the literature with a range of electron donors.[8,9,48−50,53,54] This range of donors and the complexity of the microbial interactions may help to explain why previous studies have suggested different dominant mechanisms[8,9,48−50,53,54] and why it is difficult to predict the efficacy of nitrate in the field. The efficacy of an inhibitor relies on its ability to persist in the reservoir at effective concentrations over a bioactive zone defined by temperature and electron donor availability. If the inhibitor is consumed but there is still sufficient electron donor available to reduce sulfate, then the inhibitor will simply push the zone of sulfidogenesis further into the reservoir.[54,55]

Future Modeling Directions. The examples presented here illustrate how models can be used to gain insight into the competing mechanisms controlling reservoir souring, prevention, and treatment. This is an important use of models, and the type of approach we outline should be applied more widely in souring studies to thoroughly test and explore our understanding of processes. This will allow souring models to be more than a predictive tool, generating testable hypotheses and highlighting areas where we currently need greater understanding and model-parameter constraints.

It should be noted that our current model does have limitations. A fundamental question in modeling is the level of complexity required to represent realistic systems. Overly simple representations do not always capture the dynamics of a system, while too much complexity can lead to a large number of parameters and processes that would lead to challenges in realistically constraining the system. In the interest of improving the accuracy of simulating field-scale reservoir souring and predicting the impacts of different treatment and prevention options, we look to the caveats of the current model and suggest focus areas worthy of exploring in more complexity.

Here, we assumed that the diverse sulfate reducing community can be effectively represented by a single sulfate reducing microorganism characterized by a single set of effective kinetic parameters: maximum growth rate and half-saturation constant for electron acceptors and donors. These kinetics-parameter values are assumed to be constant across all treatments (no treatment and nitrate and perchlorate treatments). This does not necessarily represent a sulfate reducing community likely to emerge in situ, which can be made up of different sulfate reducing families, each with different physiologies. Analysis of the microbial community within the columns by Engelbrektson et al.[11] revealed that different treatments can select for or inhibit different microbial taxa. To better capture the microbial community dynamics, we look toward incorporating a trait-based modeling approach, where microbial communities are divided into metabolically and functionally important groups (guilds) defined by a collection of physiological traits.[56,57] These traits, and the biochemical trade-offs between traits, determine the fitness of the guilds as a function of the environment and species interactions.

Secondly, the columns modeled in this study were isothermal, which is unlikely to be the case for reservoir environments where the injection of relatively cold water can create large temperature gradients. SRM catalyze the reduction of sulfate to sulfide via the action of intracellular enzymes. Due to the temperature sensitivity of the enzymes, SRM activities are impacted by the reservoir thermal regime. SRM have been classified according to their temperature optima into three groups (mesophiles (20−40 °C), thermophiles (40−80 °C), and hyperthermophiles (80−113 °C)) in a recent modeling study.[18] Temperature functions that modulate SRM growth rate[58,59] and trait-based modeling are therefore the next steps in

DOI: 10.1021/acs.est.6b00081
Environ. Sci. Technol. 2016, 50, 7010−7018

modeling complexity worthy of exploration in the context of microbial souring.

■ ASSOCIATED CONTENT

Supporting Information

The Supporting Information is available free of charge on the ACS Publications website at DOI: 10.1021/acs.est.6b00081.

Tables showing aqueous chemical species concentrations in Initial Water (IW) and Amendment Water (AW) for all three modeling cases, microbial and iron sulfide reactions modeled, kinetic and thermodynamic parameters of reactions, inhibition constants of reactions, and initial biomass concentrations. Additional details on microbial reactions and energetics and thermodynamic limitations on microbial reaction rates. (PDF)

■ AUTHOR INFORMATION

Corresponding Author

*E-mail: yiweicheng@lbl.gov.

Notes

The authors declare no competing financial interest.

■ ACKNOWLEDGMENTS

This work was funded by the Energy Biosciences Institute. We acknowledge the associate editor, Dr. T. David Waite, for handling this manuscript and the four anonymous reviewers for their constructive reviews that have improved the manuscript.

■ REFERENCES

(1) Machel, H. G. Bacterial and thermochemical sulfate reduction in diagenetic settings − old and new insights. *Sediment. Geol.* **2001**, *140*, 143−175.

(2) Fuller, D. C.; Suruda, A. J. Occupationally related hydrogen sulfide deaths in the United States from 1984 to 1994. *J. Occup. Environ. Med.* **2000**, *42*, 939−942.

(3) Vance, I.; Thrasher, D. R. Reservoir souring mechanisms and prevention in *Petroleum Microbiology*; Ollivier, B., Magot, M., Eds.; ASM Press: Washington, DC, 2005; pp 123−142.

(4) Semcrude. Rose Rock Daily Price Bulletin. http://crudeoilpostings.semgroupcorp.com (accessed Jan 2011).

(5) Voordouw, G.; Grigoryan, A. A.; Lambo, A.; Lin, S.; Park, H. S.; Jack, T. R. Sulfide remediation by pulsed injection of nitrate into a low temperature Candian heavy oil reservoir. *Environ. Sci. Technol.* **2009**, *43*, 9512−9518.

(6) Hubert, C. Microbial ecology of oil reservoir souring and its control by nitrate injection. In *Handbook of Hydrocarbon and Lipid Microbiology*; Timmis, K., Ed.; Springer: Berlin, Germany, 2010; pp 2753−2766.

(7) Gieg, L.; Jack, T.; Foght, J. Biological souring and mitigation in oil reservoirs. *Appl. Microbiol. Biotechnol.* **2011**, *92*, 263−282.

(8) Callbeck, C. M.; Agrawal, A.; Voordouw, G. Acetate production from oil under sulfate-reducing conditions in bioreactors injected with sulfate and nitrate. *Appl. Environ. Microbiol.* **2013**, *79*, 5059−5068.

(9) Hubert, C.; Voordouw, G. Oil field souring control by nitrate-reducing Sulfurospirillum spp. that outcompete sulfate reducing bacteria for organic electron donors. *Appl. Environ. Microbiol.* **2007**, *73* (8), 2644−2652.

(10) Haghshenas, M.; Sepehrnoori, K.; Bryant, S.; Farhadinia, M. Modeling and simulation of nitrate injection for reservoir souring remediation. *SPE International Symposium on Oilfield Chemistry* **2011**, DOI: 10.2118/141590-MS.

(11) Engelbrektson, A.; Hubbard, C. G.; Piceno, Y.; Boussina, A.; Jin, Y. T.; Wong, H.; Carlson, H.; Conrad, M. E.; Anderson, G.; Coates, J. D.; Tom, L. M. Inhibition of microbial sulfate reduction in a flow-through column system by (per)chlorate treatment. *Front. Microbiol.* **2014**, DOI: 10.3389/fmicb.2014.00315.

(12) Gregoire, P.; Engelbrektson, A.; Hubbard, C. G.; Metlagel, Z.; Csencsits, R.; Auer, M.; Conrad, M. E.; Thieme, J.; Northrup, P.; Coates, J. D. Control of sulfidogenesis through bio-oxidation of H_2S coupled to (per)chlorate reduction. *Environ. Microbiol. Rep.* **2014**, *6*, 558.

(13) Liebensteiner, M. G.; Tsesmetzis, N.; Stams, A. J.; Lomans, B. P. Microbial redox processes in deep subsurface environments and the potential application of (per)chlorate in oil reservoirs. *Front. Microbiol.* **2014**, *5*, 428.

(14) Carlson, H.; Kuehl, J.; Hazra, A.; Justice, N.; Stoeva, M.; Sczesnak, A.; Mullan, M.; Iavarone, A.; Engelbrektson, A.; Price, M.; Deutschbauer, A.; Arkin, A.; Coates, J. Mechanisms of direct inhibition of the respiratory sulfate-reduction pathway by (per)chlorate and nitrate. *ISME J.* **2015**, *9*, 1−11.

(15) Ligthelm, D. J.; de Boer, R. B.; Brint, J. F.; Schulte, W. M. Reservoir Souring: An Analytical Model for H2S Generation and Transportation in an Oil Reservoir Owing to Bacterial Activity. Paper SPE 23141. In Proceedings of Offshore Europe, Aberdeen, Scotland, Sept 3−6 1991; Society of Petroleum Engineers: Richardson, TX, 1991.

(16) Eden, B.; Laycock, P. J.; Fielder, M. *Oilfield Reservoir Souring*. HSE Books: Suffolk, England, 1993.

(17) Coombe, D.; Jack, T.; Voordouw, G.; Zhang, F.; Clay, B.; Miner, K. Simulation of Bacterial Souring Control in an Albertan Heavy Oil Reservoir. *J. Can. Petrol. Technol.* **2010**, *49*, 19−26.

(18) Farhadinia, M. A.; Bryant, S. L.; Sepehrnoori, K.; Delshad, M. Development and implementation of a multidimensional reservoir souring module in a chemical flooding simulator. *Pet. Sci. Technol.* **2010**, *28* (6), 535−546.

(19) Haghshenas, M.; Sepehrnoori, K.; Bryant, S.; Farhadinia, M. A. Modeling and simulation of nitrate injection for reservoir souring remediation. *Soc. Petrol. Eng. J.* **2012**, *17*, 817−827.

(20) Druhan, J. L.; Steefel, C. I.; Molins, S.; Williams, K. H.; Conrad, M. E.; DePaolo, D. J. Timing the onset of sulfate reduction over multiple subsurface acetate amendments by measurement and modeling of sulfur isotope fractionation. *Environ. Sci. Technol.* **2012**, *46* (16), 8895−8902.

(21) Druhan, J. L.; Steefel, C. I.; Conrad, M. E.; DePaolo, D. J. A large column analog experiment of stable isotope variations during reactive transport: I. A comprehensive model of sulfur cycling and $\delta^{34}S$ fractionation. *Geochim. Cosmochim. Acta* **2014**, *124*, 366−393.

(22) Hubbard, C. G.; Cheng, Y.; Engelbrekston, A.; Druhan, J.; Li, L.; Ajo-Franklin, J.; Coates, J. D.; Conrad, M. E. Isotopic insights into microbial sulfur cycling in oil reservoirs. *Front. Microbiol.*, **2014**, 5(480), DOI:10.3389/fmicb.2014.00480.

(23) Sonnenthal, E.; Ito, A.; Spycher, N.; Yui, M.; Apps, J.; Sugita, Y.; Conrad, M.; Kawakami, S. Approaches to modeling coupled thermal, hydrological, and chemical processes in the Drift Scale Heater Test at Yucca Mountain. *International Journal of Rock Mechanics and Mining Sciences.* **2005**, *42*, 698−719.

(24) Spycher, N. F.; Sonnenthal, E. L.; Apps, J. A. Fluid flow and reactive transport around potential nuclear waste emplacement tunnels at Yucca Mountain, Nevada. *J. Contam. Hydrol.* **2003**, *62*−*63*, 653−673.

(25) Li, L.; Steefel, C. I.; Kowalsky, M. B.; Englert, A.; Hubbard, S. S. Effects of physical and geochemical heterogeneities on mineral transformation and biomass accumulation during biostimulation experiments at Rifle, Colorado. *J. Contam. Hydrol.* **2010**, *112*, 45−63.

(26) Wanner, C.; Sonnenthal, E. Assessing the control on the effective kinetic Cr isotope fractionation factor: A reactive transport approach. *Chem. Geol.* **2013**, *337*−*338*, 88−98.

(27) Aradóttir, E. S. P.; Sonnenthal, E. L.; Björnsson, G.; Jónsson, H. Multidimensional reactive transport modeling of CO_2 mineral sequestration in basalts at the Hellisheidi geothermal field, Iceland. *Int. J. Greenhouse Gas Control* **2012**, *9*, 24−40.

(28) Xu, T.; Apps, J. A.; Pruess, K. Reactive geochemical transport simulation to study mineral trapping for CO_2 disposal in deep arenaceous formations. *J. Geophys. Res.* **2003**, *108* (B2), 2071.
(29) Xu, T.; Sonnenthal, E.; Bodvarsson, G. A reaction-transport model for calcite precipitation and evaluation of infiltration-percolation fluxes in unsaturated fractured rock, J. *J. Contam. Hydrol.* **2003**, *64* (1−2), 113−127.
(30) Xu, T.; Apps, J. A.; Pruess, K. Numerical simulation of CO_2 disposal by mineral trapping in deep aquifers. *Appl. Geochem.* **2004**, *19*, 917−936.
(31) Steefel, C.; Appelo, C.; Arora, B.; Jacques, D.; Kalbacher, T.; Kolditz, O.; Lagneau, V.; Lichtner, P.; Mayer, K.; Meeussen, J.; Molins, S.; Moulton, D.; Shao, H.; Simunek, J.; Spycher, N.; Yabusaki, S.; Yeh, G. Reactive transport cods for subsurface environmental simulation. *Comput. Geosci.* **2015**, *19*, 445.
(32) Xu, T.; Sonnenthal, E. L.; Spycher, N.; Pruess, K. TOUGHREACT - A simulation program for non-isothermal multiphase reactive geochemical transport in variably saturated geologic media: Applications to geothermal injectivity and CO_2 geological sequestration. *Comput. Geosci.* **2006**, *32* (2), 145−165.
(33) Xu, T.; Spycher, N.; Sonnenthal, E.; Zhang, G.; Zheng, L.; Pruess, K. TOUGHREACT Version 2.0: A simulator for subsurface reactive transport under non-isothermal multiphase flow conditions. *Comput. Geosci.* **2011**, *37*, 763−774.
(34) Xu, T.; Senger, R.; Finsterle, S. Corrosion-induced gas generation in a nuclear waste repository: Reactive geochemistry and multiphase flow effects. *Appl. Geochem.* **2008**, *23*, 3423−3433.
(35) Xu, T.; Pruess, K. Modeling multiphase fluid flow and reactive geochemical transport in variably saturated fractured rocks: 1. Methodology. *Am. J. Sci.* **2001**, *301*, 16−33.
(36) Pruess, K.; Oldenburg, C.; Moridis, G. *TOUGH2 User's Guide*, version 2.0; Report LBL-43134; Lawrence Berkeley National Laboratory: Berkeley, California, 1999.
(37) Singleton, M. J.; Sonnenthal, E. L.; Conrad, M. E.; DePaolo, D. J.; Gee, G. W. Multiphase reactive transport modeling of stable isotope fractionation in unsaturated zone pore water and vapor: Application to seasonal infiltration events at the Hanford Site, WA. *Vadose Zone J.* **2004**, *3*, 775−785.
(38) Rittman, B. E.; MaCarty, P. L. Environmental biotechnology: principles and applications; McGraw-Hill: New York, 2001.
(39) Maggi, F.; Gu, C.; Riley, W. J.; Hornberger, G. M.; Venterea, R. T.; Xu, T.; Spycher, N.; Steefel, C.; Miller, N. L.; Oldenburg, C. M. A mechanistic treatment of the dominant soil nitrogen cycling processes: Model development, testing and application. *J. Geophys. Res.* **2008**, *113*, G02016.
(40) Tamimi, A.; Rinker, E.; Sandall, O. Diffusion coefficients for hydrogen sulfide, carbon dioxide, and nitrous oxide in water over temperature range 293−368 K. *J. Chem. Eng. Data* **1994**, *39*, 330−332.
(41) Waybrant, K. R.; Ptacek, C. J.; Blowes, D. W. Treatment of mine drainage using permeable reactive barriers: column experiments. *Environ. Sci. Technol.* **2002**, *36*, 1349−1356.
(42) Guo, Q.; Blowes, D. W. Biogeochemistry of two types of permeable reactive barriers, organic carbon and iron-bearing organic carbon for mine drainage treatment: Column experiments. *J. Contam. Hydrol.* **2009**, *107*, 128−139.
(43) Gibson, B. D.; Amos, R. T.; Blowes, D. W. $^{34}S/^{32}S$ Fractionation during sulfate reduction in groundwater treatment systems: Reactive transport modeling. *Environ. Sci. Technol.* **2011**, *45*, 2863−2870.
(44) Poulton, S. W.; Krom, M. D.; Raiswell, R. A revised scheme for the reactivity of iron (oxyhydr)oxide minerals towards dissolved sulfide. *Geochim. Cosmochim. Acta* **2004**, *68* (18), 3703−3715.
(45) Fang, Y. L.; Yabusaki, S. B.; Morrison, S. J.; Amonette, J. P.; Long, P. E. Multicomponent reactive transport modeling of uranium bioremediation field experiments. *Geochim. Cosmochim. Acta* **2009**, *73*, 6029−6051.
(46) Li, L.; Steefel, C. I.; Williams, K. H.; Wilkins, M. J.; Hubbard, S. S. Mineral transformation and biomass accumulation associated with uranium bio-remediation at Rifle, Colorado. *Environ. Sci. Technol.* **2009**, *43*, 5429−5435.
(47) Hansel, C. M.; Benner, S. G.; Neiss, J.; Dohnalkova, A.; Kukkadapu, R. K.; Fendorf, S. Secondary mineralization pathways induced by dissimilatory iron reduction of ferrihydrite under advective flow. *Geochim. Cosmochim. Acta* **2003**, *67* (16), 2977−2992.
(48) Hubert, C.; Nemati, M.; Jenneman, G.; Voordouw, G. Containment of biogenic sulfide production in continuous up-flow-packed-bed bioreactors with nitrate or nitrite. *Biotechnol. Prog.* **2003**, *19*, 338−345.
(49) Kaster, K.; Grigoriyan, A.; Jennneman, G.; Voordouw, G. Effect of nitrate and nitrite on sulfide production by two thermophile, sulfate-reducing enrichments from an oil field in the North Sea. *Appl. Microbiol. Biotechnol.* **2007**, *75*, 195−203.
(50) Grigoryan, A.; Cornish, S.; Buziak, B.; Lin, S.; Cavallaro, A.; Arensdorf, J.; Voordouw, G. Competitive oxidation of volatile fatty acids by sulfate-and nitrate reducing bacteria from an oil field in Argentina. *Appl. Environ. Microbiol.* **2008**, *74* (14), 4324−4335.
(51) Lambo, A.; Noke, K.; Larter, S.; Voordouw, G. Competitive, microbially-mediated reduction of nitrate with sulfide and aromatic oil components in a low temperature, Western Canadian oil reservoir. *Environ. Sci. Technol.* **2008**, *42* (23), 8941−8946.
(52) Tang, K.; An, S.; Nemati, M. Evaluation of autotrophic and heterotrophic processes in biofilm reactors used for removal of sulfide, nitrate and COD. *Bioresour. Technol.* **2010**, *101* (21), 8109−8118.
(53) Hubert, C.; Voordouw, G.; Mayer, B. Elucidating microbial processes in nitrate- and sulfate-reducing systems using sulfur and oxygen isotope ratios: The example of oil reservoir souring control. *Geochim. Cosmochim. Acta* **2009**, *73*, 3864−3879.
(54) Callbeck, C.; Dong, X.; Chatterjee, I.; Agrawal, A.; Caffrey, S.; Sensen, C.; Voordouw, G. Microbial community succession in a bioreactor modeling a souring low-temperature oil reservoir subjected to nitrate injection. *Appl. Microbiol. Biotechnol.* **2011**, *91*, 799.
(55) Agrawal, A.; Park, H.; Nathoo, S.; Gieg, L.; Jack, T.; Miner, K.; Ertmoed, R.; Benko, A.; Voordouw, G. Toluene depletion in produced oil contributes to souring control in a field subjected to nitrate injection. *Environ. Sci. Technol.* **2012**, *46*, 1285−1292.
(56) Allison, S. D. A trait-based approach for modeling microbial litter decomposition. *Ecology Letters.* **2012**, *15*, 1058−1070.
(57) Bouskill, N. J.; Tang, J.; Riley, W.; Brodie, E. L. Trait-based representation of biological nitrification: model development, testing, and predicted community composition. *Front. Microbiol.* **2012**, DOI: 10.3389/fmicb.2012.00364.
(58) Ratkowsky, D.; Lowry, R. K.; McMeekin, T. A.; Stokes, A. N.; Chandler, R. E. Model for bacterial culture growth rate throughout the entire biokinetic temperature range. *J. Bacteriol.* **1983**, *154*, 1222−1226.
(59) Rosso, L.; Lobry, J. R.; Bajard, S.; Flandrois, J. P. Convenient model to describe the combined effects of temperature and pH on microbial growth. *Appl. Environ. Microbiol.* **1995**, *62* (2), 610−616.

DOI: 10.1021/acs.est.6b00081
Environ. Sci. Technol. 2016, 50, 7010−7018